ACS EARTH AND SPACE CHEMISTRY

Article

Cite This: ACS Earth Space Chem. 2019, 3, 390−402

http://pubs.acs.org/journal/aesccq

Properties of Hydrous Aluminosilicate Melts at High Pressures

Suraj K. Bajgain,[†] Ye Peng,[†] Mainak Mookherjee,*[,†] Zhicheng Jing,[‡] and Matthew Solomon[†]

[†]Department of Earth, Ocean and Atmospheric Sciences, Florida State University, Tallahassee, Florida 32306, United States

[‡]Department of Earth and Space Sciences, Southern University of Science and Technology, Shenzhen, Guangdong 518055, People's Republic of China

Supporting Information

ABSTRACT: In this study, we use *first-principles* molecular dynamics simulations to explore the behavior of anhydrous aluminosilicate melt with a stoichiometry of $NaAlSi_2O_6$ up to pressures of ∼30 GPa and temperatures between 2500 and 4000 K. We also examine the effect of water (∼4 wt % H_2O) on the equation of state and transport properties of the aluminosilicate melt and relate them to atomistic scale changes in the melt structure. Our results show that water reduces the density and bulk modulus of the anhydrous melt. However, the pressure derivative of the bulk modulus of the hydrous melt is larger than that of the anhydrous melt. The pressure dependence of the transport property exhibits an anomalous behavior. At a pressure of ∼12 GPa, anhydrous aluminosilicate melts exhibit maxima in diffusion and minima in viscosity. Dissolved water in melts also affects both diffusion and viscosity. In hydrous aluminosilicate melts, the maxima in diffusion and the minima in viscosity occur at ∼14 GPa. The anomalous behavior of transport properties is related to the pressure-induced changes in the melt structure. At shallower depths, i.e., up to 100 km, relevant for subduction zone settings, the lower density compounded by the lower viscosity of hydrous aluminosilicate melts is likely to provide buoyancy for upward migration. At greater depths of ∼180−200 km, greater compressibility of the hydrous aluminosilicate melts together with the minimum viscosity could hinder magma migration and may explain the presence of a partial melt layer at the lithosphere−asthenosphere boundary.

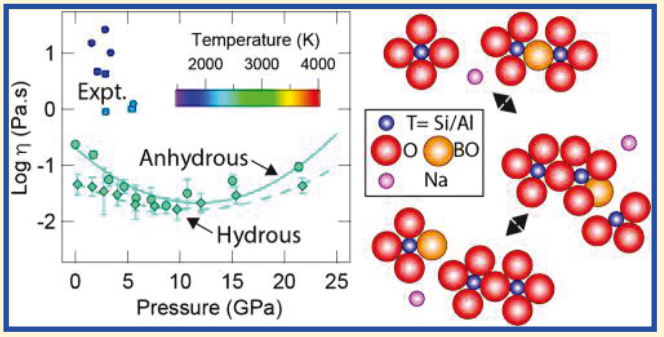

KEYWORDS: *hydrous aluminosilicate melt, high pressures, first-principles molecular dynamics, diffusion, viscosity, melt mobility*

INTRODUCTION

Melting is an important geological process, causing geochemical differentiation. In the present-day Earth, melts occur in various tectonic settings, including divergent settings, such as mid-ocean ridges (silica-poor mafic melts), convergent settings, such as subduction zones (with excess alumina, silica, and volatiles), and intraplate or ocean island/plume-related magmatism. Melts are also anticipated in the deeper parts of the Earth based on the reduction of shear wave velocity and elevated electrical conductivity. It is expected that a layer of partial melt could exist at the boundary between the lithosphere and asthenosphere,[1−4] separating the mechanically brittle lithosphere from the weaker asthenosphere. Are these melts neutrally buoyant at these depths or are they less dense than the surrounding? The mobility of the magma at these depths is controlled by the contrast in the density of the melt and the surrounding rock and also by the viscosity of the melt. Both of these physical parameters are largely influenced by the pressure, temperature, and composition, i.e., silica and/or volatile contents of the melt.

On the basis of geophysical observations, such as low shear wave velocity and elevated electrical conductivity,[5] partial melt layers are also expected at the top and bottom of the transition zone.[6,7] This is primarily owing to the large differences in the water storage capacity of the upper mantle, transition zone, and lower mantle minerals. Owing to a significantly lower water storage capacity of the major upper mantle minerals compared to the transition zone minerals, upwelling of the mantle might lead to a hydrated partially molten layer at the top of the transition zone.[8−10] However, such hydrated partial melt layers are unlikely to be global and are often observed in localized regions. As the downgoing slabs enter the lower mantle, the contrast in water storage capacity between the transition zone minerals and the very low water retention capacity in major lower mantle minerals could lead to hydrous partial melting at 660 km depths.[7] On the basis of the relationship between the mantle geotherm and the liquidus temperature of the mantle rocks, melts are also likely to be present in the core mantle boundary.[11]

In the earlier history of the Earth, i.e., magma-ocean stage, widespread silicate melting across the entire depth range of the mantle might have been more prevalent. To understand where

Received: October 16, 2018
Revised: January 19, 2019
Accepted: February 8, 2019
Published: February 8, 2019

DOI: 10.1021/acsearthspacechem.8b00157
ACS Earth Space Chem. 2019, 3, 390−402

and how the crystallization of the magma occurred, it is important to understand the inter-relationship between the geothermal gradient of the Earth in the magma-ocean stage and the liquidus temperature. The geothermal gradient in the magma-ocean stage is influenced by thermodynamic parameters, such as the Grüneisen parameter (γ), which, in turn, depends upon the pressure-dependent structural transitions in the melt.[12] Thus, it is evident that a better understanding of the atomistic scale structure of the melt in terms of the aluminosilicate network, i.e., the degree of polymerization and how it is influenced by pressure, temperature, and chemistry (silica, alumina, and water contents), will help us to have a better understanding of the deep-Earth melting processes. The degree of polymerization of silicate melts influences thermodynamic and physical properties, including compression behavior and viscosity. The ratio of non-bridging oxygen atoms (NBO) to the network-forming cations, i.e., NBO/T (where T = Al and Si), of the silicate melts shows the degree of polymerization in melts. The polymerized melts have a NBO/T ratio of <1, whereas the depolymerized melts have a NBO/T ratio of ≥2. Aluminosilicate melts are highly polymerized, with very low concentrations of non-bridging oxygen atoms. For highly polymerized aluminosilicate melts, the pressure dependence of viscosity exhibits anomalous behavior; i.e., it initially decreases with pressure, and upon further compression, viscosity increases. Similarly, the self-diffusivity of network-forming cations (silicon and aluminum) and oxygen atoms increases upon compression, and then with a further increase in the pressure, the self-diffusivity reduces.[13−20] The anomalous transport properties, i.e., the minimum in viscosity with a corresponding maximum in self-diffusion, indicate that the polymerized silicate melt could become more mobile with increasing depth.

For the depolymerized melts, upon compression, the viscosity of the depolymerized melts first increases with pressure and then decreases.[21,22] However, recent studies on silica-poor depolymerized melts show that the viscosity first decreases with the pressure.[23] In this recent study, the pressure dependence of viscosity was not at a constant temperature and, hence, may have affected the results. In yet another recent study on peridotite melt,[24] it was found that, for a constant pressure, the viscosity of the melt first increases and then decreases, similar to earlier results.[22] To illustrate the effect of the temperature, the viscosity of depolymerized melts was estimated along the melting curve and the viscosity decreased upon compression,[24] in agreement with previous studies.[23] Clearly, the transport property is sensitive to the degree of polymerization, chemistry, temperature, and pressure.

Dissolved water (H_2O) in aluminosilicate melts is likely to influence the atomistic scale structure and, in turn, influence the self-diffusion of the network-forming ions and viscosity. On the basis of low-pressure experimental studies, it is well-known that water depolymerizes the melt and, thus, enhances the viscosity and mobility of the melt.[25−27] However, the effects of water on the aluminosilicate melt at high pressure and the combined effect of water and pressure on the transport property remain poorly understood.

In this study, we use *first-principles* molecular dynamics (FPMD) simulations to explore the equation of state, self-diffusivity, and viscosity of anhydrous and hydrous aluminosilicate melts. We also relate the pressure- and temperature-dependent changes in the melt properties to the atomistic scale changes in the melt structure. In particular, we explore anhydrous aluminosilicate melts with $NaAlSi_2O_6$ stoichiometry, which resembles the stoichiometry of the crystalline mineral phase of jadeite, a high-pressure polymorph of sodic pyroxene. Molecular dynamics simulations have been quite successful in exploring the compressibility and transport properties of silicate melts with diverse chemistry, including but not limited to silica (SiO_2),[28] liquids along MgO−SiO_2,[29] natural silicate melts,[30] anorthite ($CaAl_2Si_2O_8$),[31] and anhydrous jadeite ($NaAlSi_2O_6$).[32] However, most of these previous FPMD studies explored an extended pressure range up to the core−mantle boundary pressures, i.e., ∼0−140 GPa. However, the low-pressure regimes, where these aluminosilicate melts are more likely to be relevant and often exhibit anomalous transport properties, were poorly sampled, except for a few studies.[29,30] In this study, we have explored pressures up to 30 GPa, i.e., the upper part of the lower mantle, to capture the high-pressure trends in the transport properties. However, we have also made denser samplings for pressures relevant to the crust and upper mantle conditions, i.e., up to 10 GPa.

METHODS

We used FPMD simulations as implemented in the Vienna *ab initio* simulation package (VASP)[33−35] to explore the atomistic scale structure, compressibility, thermodynamics, and transport properties of aluminosilicate melts with $NaAlSi_2O_6$ and $NaAlSi_2O_6$ with ∼4 wt % H_2O compositions. The FPMD simulations used in our study are based on local density approximation (LDA). We also used the projector augmented wave (PAW) method, as implemented in VASP.[36] We used a plane wave cutoff of 400 eV with a time step of 0.5 fs (10^{-15} s). All calculations are based on a *NVT* ensemble with a constant temperature maintained using a Nosé thermostat.[37]

A cubic cell consisting of eight $NaAlSi_2O_6$ formula units (80 atoms) was melted at 8000 K and, consequently, quenched down to the desired lower temperatures. The hydrous melt in our study consisted of four formula units of H_2O in addition to eight formula units of $NaAlSi_2O_6$, which amounts to ∼4 wt % H_2O. We examined the radial distribution function (RDF) and mean square displacement (MSD) to determine whether the atomistic scale structure is in the liquid state (see Supplementary Text S-1, Supplementary Figures S-1−S-4, and Supplementary Datasets of the Supporting Information). We computed the time averages of energy and pressure from the 20−100 ps (10^{-12} s) long simulations using the blocking method.[38] We also estimated the pressures using a higher cutoff energy of 700 eV. We corrected the average pressures obtained from the FPMD simulations using a cutoff energy of 400 eV by the additional Pulay stress term; i.e., $P = P_{400\ eV} + (P_{700\ eV} - P_{400\ eV})$. The term $(P_{700\ eV} - P_{400\ eV})$ is the volume-dependent Pulay correction and ranges between ∼3 and ∼7 GPa for the entire pressure range explored in this study. In addition to the Pulay correction, an empirical correction of 1.5 GPa is added to the pressure. The empirical correction is based on the experimental volume of jadeite melt at ambient conditions.[39−41] We adopted a similar methodology as described in detail in previous similar FPMD studies.[12,42−44]

We traced the motion of individual ions at each simulation step and used the Einstein formulation (eq 1) to estimate the self-diffusion coefficient of corresponding ions.

$$D = \lim_{n\to\infty} \frac{1}{6t}\left(\frac{1}{N}\sum_{i=1}^{N}\{r_i[t+t_0] - r_i[t_0]\}^2\right) \quad (1)$$

DOI: 10.1021/acsearthspacechem.8b00157
ACS Earth Space Chem. 2019, 3, 390−402

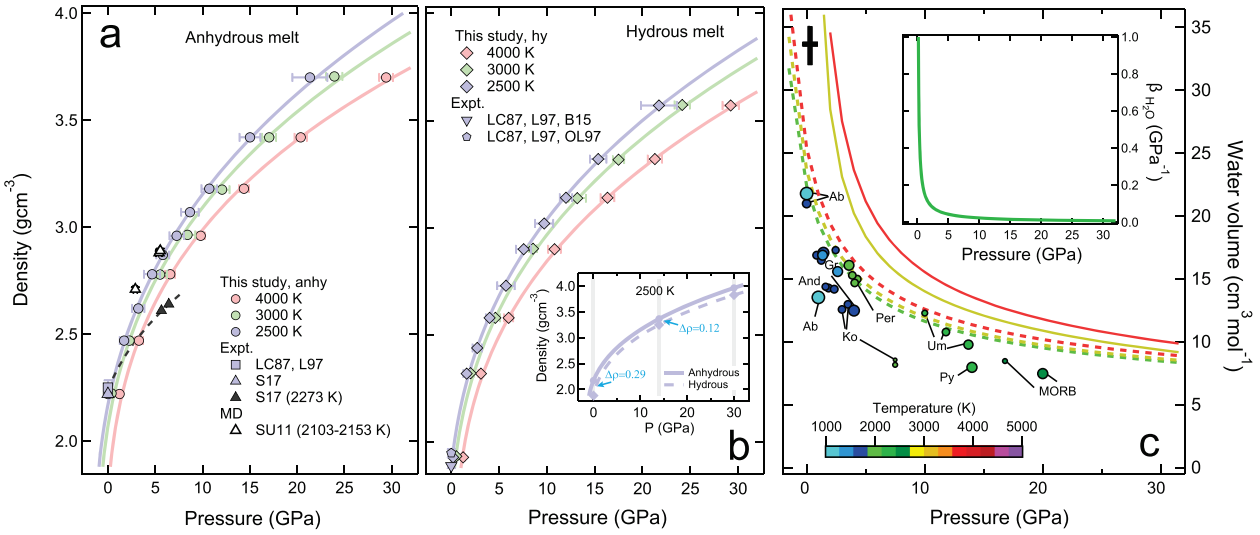

Figure 1. Pressure (P)−density (ρ) relation for (a) anhydrous and (b) hydrous aluminosilicate melts along isotherms: (light red filled symbols) 4000 K, (light green filled symbols) 3000 K, and (light blue filled symbols) 2500 K. The P−ρ data for the 2500 K isotherm (T_{ref}) could be well-described by a third-order BM equation of state formalism. The P−ρ data for all of the isotherms could then be described by a Mie Grüneisen thermal equation of state, $P(\rho, T) = P(\rho, T_{ref}) + dP/dT(T - T_{ref})$, where dP/dT ($\times 10^{-3}$, GPa/K) = 0.79 + 3505.40e$^{-11.04u}$ for anhydrous melts and dP/dT ($\times 10^{-3}$, GPa/K) = 0.61 + 449.50e$^{-7.08u}$ for hydrous melts ($u = V/V_{ref}$, where V_{ref} = 1207.95 Å^3). The thermal expansivity (α) of the hydrous melts is greater than that of the anhydrous melts at ambient pressures; i.e., $\alpha_0^{hyd} > \alpha_0^{anhyd}$. However, under compression, α decreases for both the hydrous and anhydrous melts (Supplementary Figure S-3 of the Supporting Information). Note that experimental results (LC87 and L97) on anhydrous aluminosilicate melt density are denoted by light purple filled squares. These experimental results are determined using the molar volume of oxides at 2500 K:[39,40] S17, light purple filled upward pointing triangles represent the density of the anhydrous aluminosilicate melt from the X-ray absorption experiment extrapolated to 2500 K;[41] S17 (2273 K), black filled upward pointing triangles show the density of the jadeite melt at 2273 K;[41] SU11, black open upward pointing triangles are density from classical molecular dynamics simulations at 2103−2153 K;[18] B15, light purple downward pointing triangles represent the density of the hydrous melt calculated from the partial molar volume of H_2O at 2500 K;[50] and OL97, light purple pentagons show the density of the hydrous melt calculated from the partial molar volume of H_2O at 2500 K.[49] The inset in panel b refers to the comparison between hydrous and anhydrous melt densities along the 2500 K isotherm. (c) Partial molar volume of water in the hydrous aluminosilicate melts with ∼4 wt % H_2O (dashed lines). Solid lines represent the volume of pure water.[51] Filled solid circles represent the experimentally determined partial molar volume of water in a silicate melt of diverse compositions: Ab, albite;[49,52] Ko, komatiite;[53] Um, ultramafic;[54] Per, peridotite;[55] Py, pyrolite;[56] MORB, mid-ocean ridge basalt;[57] And, andesite;[58] and Gr, granite.[59] The filled solid circles are color-coded according to the temperature. The temperature scale is shown in the bottom of the panel. The size of the filled solid symbols is proportional to the concentration of water in the melt. The smaller size represents ∼2 wt % H_2O, whereas the largest symbols represent ∼10 wt % H_2O in the melt. The maximum uncertainties associated with the presented results are shown on the left top corner of the figure. The inset in panel c shows the effect of the pressure on the compressibility (β_{H_2O}) of the H_2O component in hydrous aluminosilicate melts at 2500 K.

Table 1. Zero-Pressure Density (ρ_0), Isothermal Bulk Modulus (K_0), and First Derivative of the Bulk Modulus (K_0') of Anhydrous and Hydrous $NaAlSi_2O_6$ Melts[a]

composition (wt % H_2O)	ρ_0 (g/cm^3)	K_0 (GPa)	K_0'	temperature (K)	reference
jadeite	2.17 ± 0.08	9.70 ± 3.88	5.42 ± 1.35	2500	this study[b]
jadeite	2.25 ± 0.08[c]			2500	39 and 40
jadeite	2.20[d]			2500	41
jadeite	2.36[e]	21.50 ± 0.8	8.90 ± 1.2	1473	
jadeite (∼4)	1.88 ± 0.07	4.39 ± 1.94	6.86 ± 1.76	2500	this study[b]
jadeite (∼4)	1.95 ± 0.02[c]			2500	49
jadeite (∼4)	1.89 ± 0.01[c]			2500	50

[a]Numbers in parentheses in the first column indicate the amount of H_2O (in weight percent) for hydrous melts. [b]Third-order Birch and Murnaghan fit parameter is obtained at a constant temperature. [c]Densities are calculated using the partial molar volumes of oxide ($\bar{V}_{i,T_{ref}}$) from the experiments at reference temperature (T_{ref}) using the relation $\rho = M/\sum X_i V_i$, where X_i is the concentration of oxides, M is the total mass, and $V_i = \bar{V}_{i,T_{ref}} + d\bar{V}_i/dT(T - T_{ref})$. We used the concentration of the oxides and mass from our melt composition. $\bar{V}_{i,T_{ref}}$ and $d\bar{V}_i/dT$ for Na_2O, Al_2O_3, and SiO_2 are taken from refs 39 and 40. These parameters for H_2O are from experimental studies.[49,50] [d]Density is calculated at 2500 K using the fit parameter from the experimental study.[41] [e]The reported uncertainties in density are ∼1−2%.[41]

The component inside the parenthesis is the mean square displacement (MSD), where $r_i[t_0]$ and $r_i[t + t_0]$ are the position of the ith atom at time t_0 and its position after time t. The viscosity (η) of the aluminosilicate melt can be estimated using the Green−Kubo relation[45,46]

$$\eta = \frac{V}{10k_B}\int_0^\infty \left\langle \left(\sum_{\alpha\beta} P_{\alpha\beta}(t + t_0)P_{\alpha\beta}(t_0) \right) \right\rangle dt \quad (2)$$

where $P_{\alpha\beta}$ is the symmetrized traceless portion of the stress tensor $\sigma_{\alpha\beta}$ from each simulation step.

DOI: 10.1021/acsearthspacechem.8b00157
ACS Earth Space Chem. 2019, 3, 390−402

$$P_{\alpha\beta} = \frac{1}{2}(\sigma_{\alpha\beta} + \sigma_{\beta\alpha}) - \frac{1}{3}\delta_{\alpha\beta}\left(\sum_{\lambda}\sigma_{\lambda\lambda}\right) \quad (3)$$

In eq 3, $\delta_{\alpha\beta}$ is the Kronecker delta. We use both the off-diagonal and diagonal components of the stress tensor with different weighting factors of 1 and $^4/_3$, respectively, to calculate viscosity.[47,48] The component inside the integral is the stress autocorrelation function (ACF), which is averaged over time with different origins, t_0 (Supplementary Figure S-2 of the Supporting Information).

RESULTS

Equation of State. The pressure and volume results for the anhydrous and hydrous aluminosilicate melts can be well-explained by a third-order Birch−Murnaghan equation of state (BM3) (Figure 1 and Table 1). Our results at the 2500 K isotherm indicate that the zero-pressure density of the anhydrous aluminosilicate melt, $\rho_0^{\text{anhyd}} \sim 2.17 \pm 0.08$ g/cm^3, is ∼13% denser than the zero-pressure density of the hydrous aluminosilicate melt, $\rho_0^{\text{hyd}} \sim 1.88 \pm 0.07$ g/cm^3. Our zero-pressure densities agree well with the experimentally estimated density from the partial molar volume of oxides[39,40,49,50] (Table 1). The high-pressure experimental data determined from the X-ray absorption method[41] are quite distinct from our FPMD simulations. This discrepancy could, in part, be related to the large uncertainties associated with the X-ray absorption measurements when applied to silicate melts containing a large fraction of lighter oxide components, such as Na_2O. The very low X-ray absorption of the $NaAlSi_2O_6$ melt is not much different from the absorption by the diamond that encapsulates the melt. The surrounding pressure medium, including boron nitride (BN) and MgO, has similar and low X-ray absorption, making it challenging to correct for the background and extract the absorption as a result of the melt sample. Such technical difficulties are likely to result in uncertainties larger than a few percent and, hence, may explain the differences between the experimental results and the density predictions from FPMD simulations (Figure 1 and Table 1).

We also note that the zero-pressure bulk modulus of the anhydrous aluminosilicate melt, $K_0^{\text{anhyd}} \sim 9.70 \pm 3.88$ GPa, is more than twice the zero-pressure bulk modulus of the hydrous aluminosilicate melt, $K_0^{\text{hyd}} \sim 4.39 \pm 1.94$ GPa. While water reduces zero-pressure density and softens the zero-pressure bulk modulus of the aluminosilicate melt, it enhances the pressure derivative of the bulk modulus; i.e., $K_0'^{,\text{hyd}} > K_0'^{,\text{anhyd}}$ by ∼30% (Table 1). At pressures relevant for the upper part of the mantle transition zone, i.e., ∼14 GPa, the density difference between the hydrous and anhydrous aluminosilicate melts is reduced and is ∼3.5%. However, the density difference remains similar up to ∼30 GPa, and thus, our result does not predict the density crossover between hydrous and anhydrous melts, as suggested for ultramafic silicate melts[53] (Figure 1). In hydrous aluminosilicate melts, the H_2O component has the smallest volume among all other oxide components, i.e., Na_2O, Al_2O_3, and SiO_2. However, the H_2O component is much more compressible and, thus, plays a crucial role in determining the density of hydrous melts. We can quantify the effect of water on the density of aluminosilicate melts by analyzing the partial molar volume of water ($\bar{V}_{H_2O}$).[49,52] In the upper mantle conditions, calculated $\bar{V}_{H_2O}$ in the hydrous aluminosilicate melt is lower than the volume of pure water, V_{H_2O} (Figure 1). However, the difference between V_{H_2O} and $\bar{V}_{H_2O}$ decreases asymptotically with an increasing pressure (Figure 1). The partial molar volume of water, $\bar{V}_{H_2O}$, in the aluminosilicate melt increases with an increasing temperature at lower pressure regimes (<5 GPa), but this effect becomes temperature-insensitive at higher pressures (> ∼5 GPa) (Figure 1). This indicates that the thermal expansions for the water component in the hydrous aluminosilicate melt at lower pressures are greater and the effect of thermal expansion is reduced at higher pressures. The sharp decrease of the partial molar volume, $\bar{V}_{H_2O}$, in the aluminosilicate melt up to the pressure of ∼1 GPa can be rationalized in terms of the greater compressibility of water, $\beta_{H_2O} = -1/\bar{V}_{H_2O}(d\bar{V}_{H_2O}/dP)_T$, at these conditions (inset in Figure 1c). The H_2O component becomes stiffer at higher pressures, which is consistent with the observation that $K_0'^{,\text{hyd}} > K_0'^{,\text{anhyd}}$ (Table 1).

A comparison of $\bar{V}_{H_2O}$ from our study to a range of melt compositions from previous X-ray absorption,[55−59] sink−float methods,[53,54,56,57] and computational studies[42,43,60] shows that the partial molar volume of water in hydrous melts, $\bar{V}_{H_2O}$, is not sensitive to the melt composition, i.e., silica, alumina, mafic, and/or alkali contents. In contrast, the pressure has a significant effect on the partial molar volume of water in hydrous melts, $\bar{V}_{H_2O}$ (Figure 1 and Supplementary Figure S-3 of the Supporting Information). These comparisons also indicate that the H_2O component in all hydrous melts shows similar compression behavior with an increasing pressure. The partial molar volume of water in silicate melts is smaller than the volume of pure water up to the explored pressure range.[51] We use both the Birch−Murnaghan finite strain fit and the Vinet equation of state to define the $P-\bar{V}_{H_2O}$ relation (Supplementary Table S-1 of the Supporting Information). We find that the Vinet equation of state describes the pressure dependence of the partial molar volume of water better. The zero-pressure partial molar volume of water for jadeite (this study), $\bar{V}_{H_2O,\,0\,\text{GPa}} = 31.74 \pm 1.44$ cm^3/mol at 2500 K, is greater than the partial molar volume of water, $\bar{V}_{H_2O,\,0\,\text{GPa}} = 24.97$ cm^3/mol, for albite melt at 1273 K.[52] The equation of state fitting of four different melt compositions with NBO/T = 0.8−1.5 reported a $\bar{V}_{H_2O,\,0\,\text{GPa}}$ value of 23.8 ± 0.5 cm^3/mol at 1273 K.[50] The larger partial molar volume of water in our study is due to higher temperatures of ∼2500 K. The positive correlation between the partial molar volume of water and temperature has been well-documented across a wide variety of melt compositions.[61]

Diffusion. Diffusion of the individual ions in an aluminosilicate melt is an activated process, and the individual ions must have sufficient activation energy to diffuse. The random motions of the ions in the melt are thermally activated,[62,63] but such motion might require larger volumes as the diffusing species transition between the ground state and the activated state. Hence, owing to this activation volume, diffusion is likely to be hindered at higher pressures. An Arrhenius relation (eq 4) often adequately describes the pressure and temperature dependence of self-diffusion coefficients

$$D = D_0 \exp\left(-\frac{E^* + PV^*}{RT}\right) \quad (4)$$

where D_0 is the pre-exponential factor, E^* is the activation energy, V^* is the activation volume, and R is the gas constant.

DOI: 10.1021/acsearthspacechem.8b00157
ACS Earth Space Chem. 2019, 3, 390−402

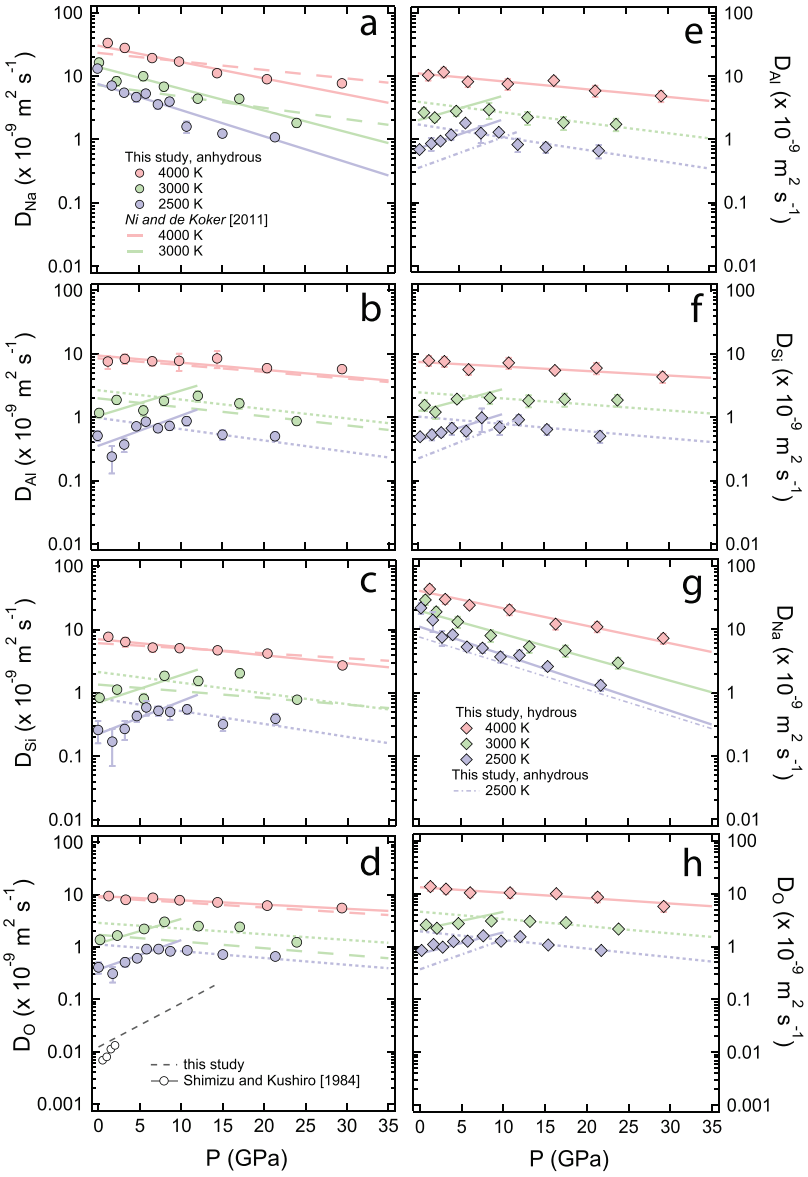

Figure 2. Plots show the pressure and temperature dependence of the self-diffusion of (a) Na, (b) Al, (c) Si, and (d) O ions for anhydrous aluminosilicate melts. Plots show the pressure and temperature dependence of the self-diffusion of (e) Na, (f) Al, (g) Si, and (h) O ions for hydrous aluminosilicate melts. Light red, light green, and light blue filled symbols represent self-diffusion at 4000, 3000, and 2500 K isotherms, respectively. Lines represent the Arrhenius fit to the FPMD data (Table 2). Dotted lines are the Arrhenius fit to the FPMD diffusion data for high-pressure regimes for Al, Si, and O ions at lower temperatures, i.e., 3000 and 2500 K. For panels a−d, dashed lines represent results at 4000 and 3000 K from an earlier FPMD study.[32] For panels e−h, dash-dot lines represent the Arrhenius fit to the FPMD self-diffusion data for the anhydrous aluminosilicate melts at 2500 K and are always lower than the self-diffusion for the hydrous aluminosilicate melts. In panel d, the black dashed line represents low-temperature extrapolation of the oxygen self-diffusion data for the anhydrous aluminosilicate melts. The extrapolation is in good agreement with previous experimental results.[68] The discrepancy in the slope, i.e., activation volume between the extrapolated results and the experiment, indicates temperature dependence of the activation volume.

Results from the FPMD simulations show that the self-diffusivities of sodium and hydrogen are among the fastest in the aluminosilicate melts (Figure 2). At 4000 K, self-diffusivity of all ionic species decreases with increasing pressure. At T of ≤3000 K, self-diffusivity of Na decreases with pressure. However, at T of ∼2500 and 3000 K, the diffusivity of Al, Si, O, and H first increases with pressures up to ∼12 GPa, and at pressures of >12 GPa, the diffusivity reduces (Figure 2). This anomalous behavior at low pressures (<12 GPa) and normal behavior at high pressures could be explained by two distinct Arrhenius relations. The low-pressure regime where the diffusivity increases with pressure yields a negative activation volume (Table 2), whereas the high-pressure regime where diffusivity is hindered yields a positive activation volume. A negative activation volume means that the activated complex is denser than the ground state[64] (Figure 2 and Table 2). At low pressures, the magnitude of the negative activation volume (V^*) shows maxima at low temperatures, i.e., at 2500 K; the magnitude of the negative activation volume (V^*) gradually reduces at high temperatures and eventually reverses to a positive activation volume (V^*) at 4000 K (Figure 2 and Table 2). Such anomalous behavior in the pressure and temperature dependence of diffusivity has been observed in polymerized aluminosilicate

DOI: 10.1021/acsearthspacechem.8b00157
ACS Earth Space Chem. 2019, 3, 390−402

Table 2. Pre-exponential Self-Diffusion Coefficient ($D_{X,0}$), Activation Energy (E^*), and Activation Volume (V^*) from the Arrhenius Fit (eq 4) for the Anhydrous $NaAlSi_2O_6$ Melts (Jadeite) and Hydrous $NaAlSi_2O_6$ Melts (Jadeite, hy).

species (X)	composition	$D_{X,0}$ ($\times 10^{-9}$, $m^2\ s^{-1}$)	E^* (kJ mol^{-1})	V^* ($cm^3\ mol^{-1}$)	reference
Na	jadeite	309 ± 32	77 ± 3	1.98 ± 0.07	this study
		786 ± 50	117 ± 8	1.03 ± 0.10	32
			90		69
	jadeite, hy	356 ± 66	72 ± 5	2.11 ± 0.14	this study
Al	jadeite	406 ± 89	125 ± 6	0.86 ± 0.13	this study[a]
		245 ± 128	136 ± 12	−2.30 ± 0.44	this study[b]
		666 ± 60	145	0.82 ± 0.10	32
			300		69
	jadeite, hy	250 ± 59	103 ± 7	0.95 ± 0.20	this study[a]
		356 ± 210	129 ± 13	−2.18 ± 0.45	this study[b]
Si	jadeite	251 ± 32	119 ± 3	0.97 ± 0.09	this study[a]
		221 ± 125	143 ± 13	−2.49 ± 0.43	this study[b]
		553 ± 20	150 ± 3	0.61 ± 0.10	32
	jadeite, hy	204 ± 49	110 ± 7	0.55 ± 0.20	this study[a]
		255 ± 164	133 ± 14	−1.98 ± 0.48	this study[b]
	enstatite, hy	250	97	2.24	70
O	jadeite	328 ± 41	118 ± 3	0.62 ± 0.08	this study[a]
		370 ± 179	144 ± 11	−2.69 ± 0.42	this study[b]
		1229	164 ± 2	0.74 ± 0.10	32
				−6.30 ± 1.20	68
	jadeite, hy	321 ± 73	106 ± 7	0.78 ± 0.17	this study[a]
		384 ± 248	130 ± 14	−1.93 ± 0.45	this study[b]
	enstatite, hy	240	94	2.24	70
H	jadeite, hy	994 ± 196	91 ± 6	0.42 ± 0.14	this study[a]
		450 ± 285	83 ± 14	−0.72 ± 0.37	this study[b]
	enstatite, hy	920	85	0.45	70

[a]Fit parameters are obtained using results from the 4000 K isotherm and the result from the high-pressure regime (~12−30 GPa) along 2500−3000 K. [b]Fit parameters are obtained from the low-pressure regime (~0−12 GPa) along 2500−3000 K.

melts with different compositions, including, silica, albite, jadeite, dacite, and basalt.[14,16,65−67]

The diffusivity of all ionic species in hydrous melts is greater than that of anhydrous melts. This finding is consistent with the fact that water enhances the melt mobility by disrupting the intermediate range melt structure.[27,71] At low pressures and 2500 K, Na diffusion is significantly greater than that of other ions; i.e., $D_{Na} \approx 10D_{Si\ or\ Al}$, for both anhydrous and hydrous aluminosilicate melts. At higher pressures of ~20 GPa, the reduction of Na diffusivity is more than that of other ions; i.e., $D_{Na} \approx 2D_{Si\ or\ Al}$. As the temperature increases, $D_{Na}/D_{Si\ or\ Al}$ becomes smaller; i.e., at higher temperatures, the diffusivity of the other ionic species increases more relative to that of Na. At the 2500 K isotherm and at pressures of up to 12 GPa, D_{Na} decreases at a higher rate compared to that at $P > 12$ GPa. The sodium (Na) cation is large in size and is weakly bonded to the oxygen ions compared to Si or Al. Thus, Na moves freely through the melt structure if space is available. This results in higher D_{Na} at lower pressures, but owing to the collapse of the free space within the aluminosilicate melt at high pressures, D_{Na} decreases more rapidly with an increasing pressure. A similar trend of D_{Na} was reported from previous classical MD simulations, although the magnitude of diffusivity predicted from classical simulations and the present results from FMPD differ significantly.[65,69] Our results for the anhydrous melt agree well with previous FPMD studies.[32]

Self-diffusion coefficients of network-forming cations, i.e., silicon and aluminum, are comparable to each other, with D_{Al} being slightly larger than D_{Si}. At 4000 K, both D_{Si} and D_{Al} decrease with increasing pressure. Along the lower isotherms, i.e., 2500 and 3000 K, D_{Si} and D_{Al} increase as a function of the pressure up to ~12 GPa, and at a pressure of >12 GPa, both D_{Si} and D_{Al} reduce upon compression (Figure 2). This anomalous pressure dependence of D_{Si} and D_{Al} is present for temperatures up to 3000 K and is lost at higher temperatures, i.e., 4000 K, where both D_{Si} and D_{Al} reduce upon compression across all pressures. Oxygen self-diffusion (D_O) exhibits a trend similar to that of both D_{Si} and D_{Al} diffusion (Figure 2). At 4000 K and ambient pressures, hydrogen is one of the fastest moving ions with the highest self-diffusion (D_H) in hydrous melts, such that $D_H \approx 2D_{Na}$. As pressure increases, D_{Na} decreases more rapidly, such that, at the highest pressure (~30 GPa) explored in this study, $D_H \approx 5D_{Na}$. However, at lower isotherms (2500−3000 K) up to ~5 GPa, $D_H \sim D_{Na}$ (Figure 3). It is very likely that hydrogen forms hydroxyl bonds with the oxygen ions and hops in between oxygen atoms. At lower pressures, we find that the hydrogen speciation is dominated by hydroxyl (OH) at ~80% and there are ~15% molecular H_2O species. At higher pressures, both hydroxyl (OH^-) and molecular H_2O reduce in abundance. Also, the hydrogen ions increasingly attach to bridging oxygen ions (−H−O−H−) (Supplementary Figure S-3 of the Supporting Information). This has also been observed in hydrous basaltic melts[43] and $MgSiO_3$ melts.[42] At the low pressures and temperatures explored in this study, the proportion of H_2O is lower compared to the experimental studies. In the experimental studies on hydrated albitic glass, the abundance of hydroxyls (OH^-) and molecular H_2O varies as a function of the total water content. At the total water concentration of ~4 wt % H_2O, hydroxyls (OH^-) and molecular H_2O in a hydrated albitic glass are equally abundant.[72] However,

DOI: 10.1021/acsearthspacechem.8b00157
ACS Earth Space Chem. 2019, 3, 390−402

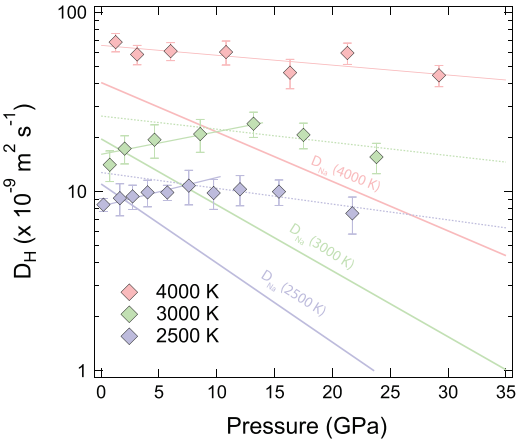

Figure 3. Plot of pressure and temperature dependence of self-diffusion data for hydrogen in hydrous aluminosilicate melts. Light red, light green, and light blue filled symbols represent self-diffusion at 4000, 3000, and 2500 K isotherms, respectively. Thin lines represent the Arrhenius fit to the FPMD self-diffusion data. Dotted lines are the fitted results using the self-diffusion coefficients from high-pressure regimes, i.e., 3000 and 2500 K. For comparison, the thick lines show the Arrhenius fit to the Na diffusion for hydrous melts.

the temperature explored in the experimental studies (~1223 K)[72,73] is significantly lower than the present study (~2500 K), which might explain the discrepancies. Lower concentrations of H_2O in the hydrous jadeite melt in high-temperature FPMD simulations (~2500 K) are consistent with the finding that OH^- largely dominates over molecular H_2O with an increasing temperature in the hydrous albite melt.[74] At temperatures lower than 3000 K, oxygen self-diffusion (D_O) shows an anomalous pressure dependence and hydrogen, owing to its association with the oxygen ions, also shows a similar behavior in hydrogen self-diffusion (D_H); hence, $D_H < D_{Na}$. The anomalous pressure dependence of D_O and D_H observed at low temperatures is lost at higher temperatures, and hence, $D_H > D_{Na}$ (Figure 3).

The activation energies of the self-diffusion for hydrous melts are smaller than those for the anhydrous melts; i.e., $E_x^{*,hyd} < E_x^{*,anhyd}$ (Table 2). For both the anhydrous and hydrous aluminosilicate melts, the activation energies (E^*) for the diffusion of network-forming cations (Si and Al) are larger than those of the network-modifying cations (Na and H) (Table 2 and Figure 2). The self-diffusivities for individual ionic species for the hydrous melts are also greater than those for the anhydrous melts; i.e., $D_x^{hyd} > D_x^{anhyd}$, where x refers to Na, Al, Si, and O ionic species. The activation volumes for the self-diffusivities of Na and O in hydrous melts are larger than those of anhydrous melts; $V_{Na/O}^{*,hyd} > V_{Na/O}^{*,anhyd}$. For the anhydrous melts, at low temperatures (i.e., 2500−3000 K) and pressures, the activation volume for oxygen diffusion, $V_O^{*,anhyd}$, is ~ −1.94 cm^3 mol^{-1}. This estimation is larger compared to the experimental activation volume[68] of −6.3 cm^3 mol^{-1} from 0 to 2 GPa and <2000 K. This is consistent with the fact that, at low pressures, the activation volume for the diffusing oxygen ions is dependent upon the temperature. The activation volume becomes larger with an increasing temperature as also observed from self-diffusion coefficients at 4000 K, which yield a positive activation volume. In low-pressure and low-temperature regimes, the activation volume for silicon diffusion, $V_{Si}^{*,anhyd}$, is ~ −2.28 cm^3

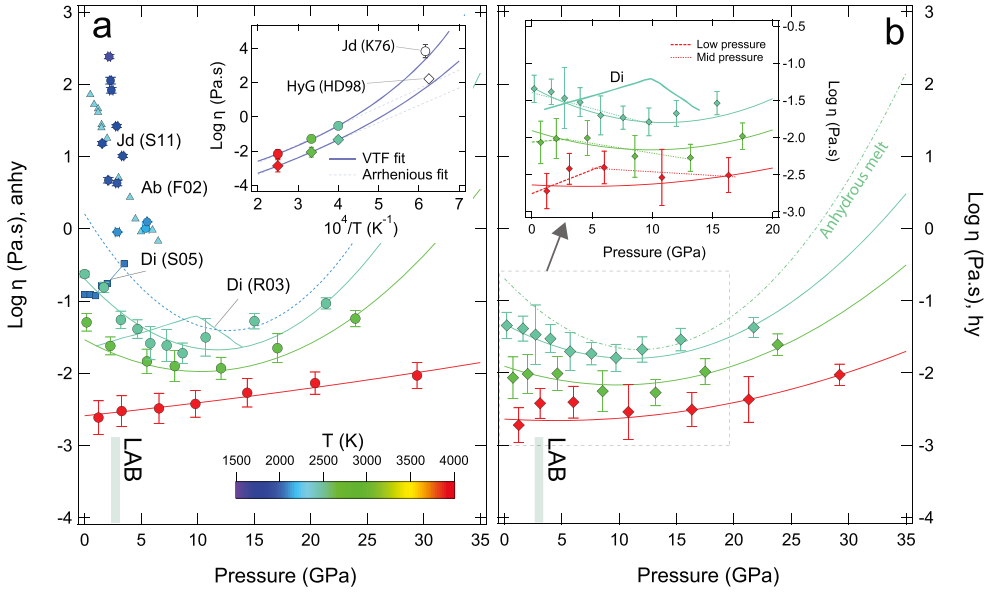

Figure 4. Plots of the pressure dependence of viscosity for (a) anhydrous and (b) hydrous melts. The viscosity is plotted on a logarithmic scale. Filled circles and rhombs represent FPMD viscosity data for anhydrous and hydrous aluminosilicate melts, respectively. The symbols are color-coded on the basis of the temperature. The temperature scale is shown in a horizontal bar at the bottom of the panel a. Lines represent the fit to the FPMD viscosity data using a modified Arrhenian relationship (eqs 6 and 7). Also shown are the experimental data for polymerized melts: Jd (S11), jadeite;[18] Ab (F02), albite;[79] and depolymerized melts: Di (R03), diopside;[22] Di (S05), diopside.[80] We use color to show the temperature of the study. The inset in panel a shows the temperature dependence of viscosity at a constant pressure (~0 GPa) for anhydrous and hydrous aluminosilicate melts. Experimental viscosity results at 0 GPa and lower temperatures are for jadeite melt[13] and granitic melt with ~4 wt % water.[76] Thin lines represent the Arrhenius relation. Thick lines show the TVF relation (Supplementary Table S-2 of the Supporting Information). The inset in panel b shows the viscosity of the hydrous melts up to 20 GPa. Thick dashed and dotted lines are the viscosity trends from Arrhenius fitting at low- and mid-pressure regimes, where global Arrhenius cannot fully describe the pressure evolution of viscosity. At higher temperatures (4000 K) and low pressure, the pressure dependence of viscosity of the hydrous aluminosilicate melts resembles that of depolymerized melts.[22]

DOI: 10.1021/acsearthspacechem.8b00157
ACS Earth Space Chem. 2019, 3, 390−402

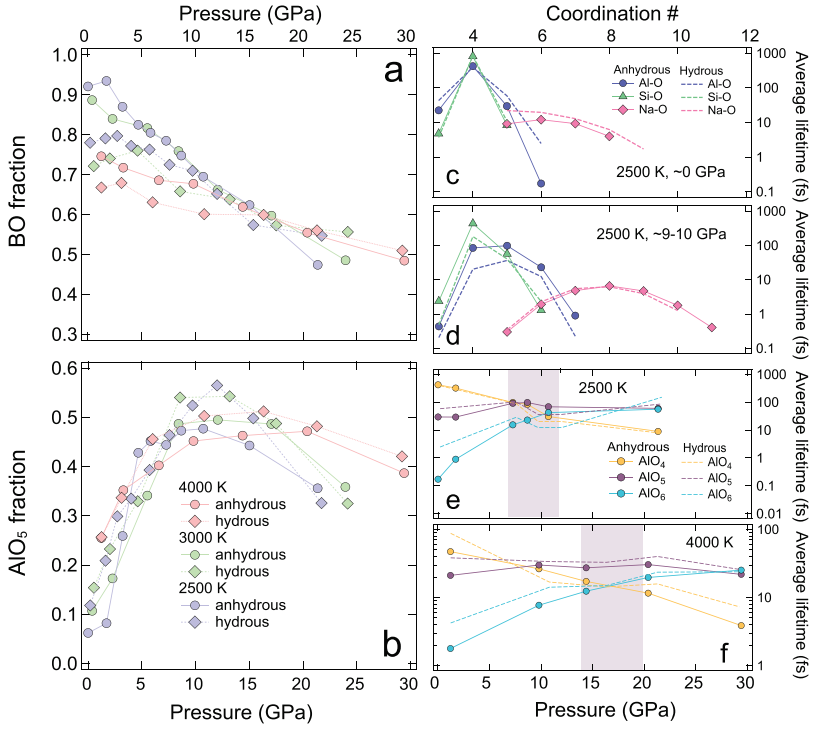

Figure 5. Plots of (a) fraction of BO and (b) five coordinated Al, AlO_5, in anhydrous (filled circles) and hydrous (filed rhombs) aluminosilicate melts. Light red, light green, and light blue filled symbols represent data at 4000, 3000, and 2500 K isotherms, respectively. Plots show the average lifetime (τ) of Al−O, Si−O, and Na−O species for anhydrous (solid lines with symbols) and hydrous (dashed lines) jadeite melt at (c) 2500 K and ambient pressures and (d) 2500 K and 9 GPa. The average lifetime (τ) is in femtoseconds and is normalized to 1 ps of simulation time. Plots of average lifetime (τ) of 4-, 5-, and 6-fold coordinated Al−O species in anhydrous melt (solid lines with circles) and hydrous melt (dashed lines) at (e) 2500 K and (f) 4000 K. The shaded regions in panels e and f represent the area where AlO_5 is most abundant.

mol^{-1}. This estimate is also smaller than the observed experimental results at ∼2100 K for the aluminosilicate melts.[14] Our results on the activation energy and activation volume of H diffusion agree well with those of the hydrous $MgSiO_3$ melt[70] (Table 2).

Viscosity. Our FPMD results indicate that the viscosity (η) of the anhydrous aluminosilicate melts with a stoichiometry of $NaAlSi_2O_6$ decreases with an increasing pressure up to 10−12 GPa. At pressures greater than 12 GPa, viscosity increases upon further compression. Thus, there occurs a pressure-dependent minimum in viscosity of the anhydrous aluminosilicate melts at around ∼12 GPa. This anomalous pressure minimum changes with the temperature; i.e., minima are more pronounced at lower temperatures and disappear at higher temperatures (4000 K). A similar behavior is also observed in the hydrous melts; however, the pressure-dependent viscosity minimum is shifted to slightly higher pressures (Figure 4). Over a temperature range of 2500−4000 K and at zero pressure, the viscosity of anhydrous and hydrous aluminosilicate melts exhibits a non-Arrhenian behavior. We have used a Tamman−Vogel−Fulcher (TVF) relation to describe the temperature dependence of the viscosity (η)

$$\eta = \eta_0 \exp\left[\frac{A}{(T - T_0)}\right] \tag{5}$$

where η_0 is the pre-exponential viscosity and A and T_0 are constants. We have also used a global Arrhenius fit to describe the pressure and temperature dependence of viscosity[31,75]

$$\eta = \eta_0 \exp\left(\frac{E^* + PV^*}{RT}\right) \tag{6}$$

where

$$V^* = (V_1 + V_2T) + P(V_3 + V_4T + V_5/T) \tag{7}$$

where η_0 is the pre-exponential viscosity and E^* is the activation energy from the viscosity fit. In the modified Arrhenius equation, the activation volume (V^*) varies as a function of the pressure and temperature (eq 6). Note that, at zero pressure, eq 6 reduces to an Arrhenius equation $\eta = \eta_0 \exp[E^*/RT]$. On the basis of our results, we note that an Arrhenius relation cannot successfully describe the temperature-dependent viscosity at zero pressure (Figure 4 and Supplementary Figure S-4 of the Supporting Information). For instance, for the anhydrous aluminosilicate melts, the viscosity predicted by the Arrhenius relation deviates from the experimental results at lower temperatures.[13] Similarly, for the hydrous melts, the viscosity predicted by the Arrhenius relation is smaller than the experimentally determined viscosity of granitic melt with ∼4 wt % H_2O.[76] In contrast, the TVF relations (eq 5) provide a better description of the variation of viscosity with the temperature (Figure 4 and Supplementary Table S-2 of the Supporting Information). The TVF relation has also been quite successful in describing the temperature dependence of the viscosity of several other polymerized melts.[19,31,77,78]

For anhydrous melts, our estimation of the activation energy (E^*) for the pressure and temperature dependence of viscosity using the modified Arrhenius fit is ∼246 kJ mol^{-1} (Supplementary Table S-2 of the Supporting Information). Previous experiments, conducted at lower temperatures (1623−2163 K)

DOI: 10.1021/acsearthspacechem.8b00157
ACS Earth Space Chem. 2019, 3, 390−402

and pressures (0−7 GPa) predicted larger activation energies of ∼370 kJ mol^{-1} for jadeite and ∼368 kJ mol^{-1} for albite at l973 K.[18,79] Larger activation energies of experimental studies indicate that the activation barrier may be large as a result of lower temperature conditions of the experiments. Comparisons between previous experiments and our simulation results indicate that the viscosity of aluminosilicate liquids increases by ∼1−3 orders of magnitude when the temperature decreases from 2500 to ∼2100−1800 K.[18]

At ambient pressure and 2500−3000 K, we find a ∼5−6-fold decrease in viscosity of anhydrous aluminosilicate as a result of ∼4 wt % H_2O in the melt (Figure 4). However, the pressure evolutions of viscosity in hydrous and anhydrous melts are quite different. For instance, anhydrous melts at 4000 K show a normal viscosity trend; i.e., viscosity increases with increasing pressure (Figure 4). At lower isotherms, viscosity decreases with increasing pressure and reaches its minimum at ∼10−12 GPa before increasing with an increasing pressure. In hydrous melts, viscosity shows a positive (normal) pressure dependence for P = ∼0−5 GPa, followed by a weak negative pressure dependence for P = ∼8−10 GPa and normal pressure behavior at higher pressures, i.e., P > 10 GPa (Figure 4). This will lead to the smallest viscosity difference between hydrous and anhydrous melts at ∼4−5 GPa. The observed viscosity trends of hydrous jadeite melt at 3000 and 4000 K are similar to those of depolymerized melts, such as diopside.[22,75] However, the viscosity trend of hydrous melts at 2500 K is the same as that of anhydrous melts with a negligible positive pressure dependence of viscosity at P < 5 GPa.

Melt Structure. The difference between the transport properties (e.g., viscosity) of anhydrous and hydrous aluminosilicate melts can be related to the atomistic scale structural differences primarily caused by dissolved H_2O. Water in the melt often acts as a network modifier; i.e., it depolymerizes the melt structure, which results in an increase in the concentration of the NBO. At ambient pressure and 2500 K, in anhydrous aluminosilicate melts, around ∼90% of oxygen ions are bridged (i.e., BO) with network-forming cations in tetrahedral (T = Si and Al) coordination. The presence of NBO is <5%, and the remaining oxygen ions often form triclusters ($O-T_3$), i.e., oxygen ions surrounded by three tetrahedral cations (Supplementary Figure S-2 of the Supporting Information). Under similar pressure and temperature conditions, hydrous aluminosilicate melts contain around ∼80% BO with network-forming tetrahedral cations (T = Si and Al) and ∼20% NBOs (Supplementary Figure S-2 of the Supporting Information and Figure 5). This shows that the addition of H_2O disrupts the polymerized chain of network-forming cations in the anhydrous melt, resulting in the high abundance of NBOs, which lowers the melt viscosity.[26,71]

We also calculated the X-ray structure factor, $S(Q)$, of anhydrous and hydrous melts using the Fourier transformation of the RDF.[81] This allows us to compare our results to available experimental data (Supplementary Figure S-1 of the Supporting Information). Our results on $S(Q)$ from FPMD simulations are in good agreement with the X-ray diffraction data obtained on the jadeite melt.[20,82] All of the structure factors show a well-defined first sharp diffraction peak (FSDP) that usually corresponds to medium-range features related to TO_4 rings.[82,83] The FSDPs at 2500 K are less intense than those of the experimental studies at 1923 and 2173 K. Results from FPMD simulations at higher temperatures are consistent with the experiments at lower temperatures and possibly indicate less abundance of the TO_4 rings at higher temperatures (Supplementary Figure S-1 of the Supporting Information).

DISCUSSION

The anomalous pressure dependence of transport properties in silicate melts has been extensively studied.[13,17,18,65,79,84] Several mechanisms have been proposed to explain this observation, which include (a) differences in the abundance of BO, (b) relative abundance and changes in the coordination number of the network-forming cation, and (c) a reduction in the intertetrahedral (T−O−T) bond angles.[14,20,85−88]

Our FPMD results on the anhydrous aluminosilicate melts are consistent with the previous studies. We do observe pressure-dependent anomalous behavior of the self-diffusivity (Figure 2) and viscosity (Figure 4), which is more pronounced at lower temperature isotherms (2500−3000 K). We note that the pressure-induced changes in the coordination of network-forming cations and the abundance of the BOs and NBOs are related. For instance, at lower temperatures, in the anhydrous aluminosilicate melts, increasing pressure leads to transformation of AlO_4 to AlO_5 by reducing the number of NBOs via the reaction $AlO_4 + NBO = AlO_5$, where AlO_5 has at least one BO. At even higher pressures, AlO_5 transforms to AlO_6 via the reaction $AlO_5 + NBO = AlO_6$, where AlO_6 has at least one BO. The NBOs could also be consumed by AlO_4 via the reaction $AlO_4 + 2NBO = AlO_6$, where AlO_6 has at least two BOs. Thus, the fraction of NBOs decreases with pressure and promotes the formation of bridging oxygen, i.e., $O-T_2$. Owing to the polymerized nature of the anhydrous melts, although the NBOs are often low in concentration, the formation of AlO_5 may be aided by BOs as in the reaction $AlO_4 + BO = AlO_5$, where AlO_5 contains an oxygen atom that is attached to three network-forming cations, i.e., an oxygen tricluster ($O-T_3$) (Supplementary Figure S-2 of the Supporting Information). The pressure dependence of the T−O−T angle at low temperatures also shows a relatively rapid reduction from ∼140° to 134°, i.e., 6° reduction between 0 and 5 GPa. This is owing to the compression being accommodated by the tilting of the polyhedral linkages. Upon further compression, a further 6° reduction occurs over a 25 GPa interval, indicating that the compression mechanism is accommodated by transformation of the polyhedral units, i.e., $TO_4 \rightarrow TO_5 \rightarrow TO_6$ (Supplementary Figures S-1 and S-2 of the Supporting Information).

The anomalous pressure dependence of the self-diffusivity and viscosity is likely to be related to the changes in the structure of the melt upon compression. We note that the network connectivity of the TO_4 units (T = Si/Al), as captured by the Q^4 and Q^3 species, is significantly reduced upon compression, and this may lead to an enhancement of viscosity. However, while the abundance of Q^4 and Q^3 species reduces with pressure, the melt polymerizes further, with the network becoming more connected, as evident from the increasing abundances of Q^5 and Q^6 species (Supplementary Figure S-2 of the Supporting Information).

One possible explanation for the observed anomalous behavior in the transport property could be related to the fact that TO_5 units are inherently less stable compared to TO_4 and TO_6, where T = Al and/or Si. This is captured by the lifetime (τ) of the species at low-temperature isotherms (2500 K), and at the lowest pressures, where AlO_4 is the dominant species, the lifetime of the species shows the following relation: $\tau_{AlO_4} \gg \tau_{AlO_5} \gg \tau_{AlO_6}$. However, at modest pressures, where AlO_5 is the

DOI: 10.1021/acsearthspacechem.8b00157
ACS Earth Space Chem. 2019, 3, 390−402

dominant species, $\tau_{AlO_4} \leq \tau_{AlO_5} \geq \tau_{AlO_6}$ (Figure 5). The relatively shorter lifetime of AlO_5 compared to AlO_4 and AlO_6 might lead to the release of an oxygen ion and/or addition of oxygen atoms to reach the stable states of AlO_4 or AlO_6, thus facilitating anomalously high diffusion and/or lower viscosity. The unstable nature and relatively shorter lifetime of AlO_5 compared to AlO_4 and AlO_6 could also be related to higher configurational entropy as well as decreases in the activation barrier of the melt transportation, i.e., lower viscosity.[14,88−92] The lifetime (τ) of the species also decreases significantly with the temperature. For instance, at 4000 K and at modest pressures, $\tau_{AlO_5} > \tau_{AlO_4} \approx \tau_{AlO_6}$. At higher temperatures, all of the species have shorter lifetimes, and while AlO_5 is unstable, AlO_4 and AlO_6 are also very unstable, owing to the enhanced temperature. Thus, at high-temperature isotherms (e.g., 4000 K), the anhydrous aluminosilicate melts exhibit normal behavior; i.e., the self-diffusivity of all of the ionic species reduces upon compression (Figure 2), and the viscosity increases upon compression (Figure 4). This is expected because the activation barrier for diffusion is expected to be lower at high temperatures and the effect of the temperature is more predominant over the atomistic scale changes in the melt structure as a result of the increase in the pressure. Also, higher temperatures (e.g., 4000 K) help in depolymerizing the aluminosilicate melts, resulting in the high abundance of NBOs (Figure 5). For instance, at 4000 K and ∼0 GPa, anhydrous aluminosilicate melts contain ∼10% NBOs, which is twice the concentration of NBOs at ambient pressures and lower temperatures, i.e., 2500−3000 K (Supplementary Figure S-2 of the Supporting Information).

The effect of water on the pressure-dependent anomalous behavior of aluminous melts with $NaAlSi_2O_6$ stoichiometry was previously unknown, and our study shows how water enhances the diffusion and reduces the viscosity. The addition of water depolymerizes the aluminosilicate melts. At low temperatures, the pressure dependence of the self-diffusivity and viscosity is similar to what has been observed in the anhydrous melts. However, owing to the depolymerizing effects of water, the anomalous behavior is pushed to 2−3 GPa higher pressures compared to the anhydrous melts. The mechanisms discussed, i.e., the unstable nature and relatively shorter lifetime of AlO_5 compared to AlO_4 and AlO_6, are also applicable to the hydrous melt. At higher temperatures (i.e., 4000 K), the hydrous melts show added complexity in the pressure evolution of self-diffusivity and viscosity at low pressures. This is primarily owing to the depolymerizing effect of both water and temperature, whereby the melt structure resembles a depolymerized melt, such as diopside.[21,22] In diopside melt, the viscosity first increases and then decreases with increasing pressure. At higher temperatures (i.e., 4000 K), we observe similar effects of first an increase in viscosity, then reduction, and then an eventual increase at further compression.

The results on compressibility and transport properties from this study are likely to help us to better understand the mobility of magma in a reservoir. For instance, in a reservoir with constant permeability (k), the velocity of the melt migration is related to the ratio of the density contrast between the melt and the surrounding rock ($\Delta\rho$) and the viscosity of the melt (η), i.e., $\Delta\rho/\eta$.[93,94] Typical mantle minerals have bulk moduli of the order of ∼100 GPa.[95,96] Silicate melts are much more compressible, i.e., ∼5−10 times more compressible, than the mantle minerals because their bulk moduli range from ∼10 to 25 GPa but often have larger pressure derivatives.[57,97,98] This leads to a large $\Delta\rho$ with an increasing pressure. The ascending magma experiences an increase in buoyancy caused by the large $\Delta\rho$. The buoyancy of the magma will be enhanced if the melt is hydrous because this further lowers the melt density. However, on the basis of our results, the pressure derivative of the bulk modulus of hydrous aluminosilicate melts is larger than that of anhydrous melts; i.e., $K_0'^{,hyd} > K_0'^{,anhyd}$. This is also captured in the relatively rapid reduction of β_{H_2O} at pressures of <1 GPa and reduces moderately until pressures of ∼3 GPa. Thus, a hydrous aluminosilicate magma generated at depths of less than 30−90 km will have a large $\Delta\rho$. However, the effect of large buoyancy, owing to hydrous melts, will reduce significantly beyond ∼100 km depths. Thus, for both hydrous and anhydrous melts, $\Delta\rho$ reduces significantly at depths greater than ∼100 km, rendering a lower melt velocity, owing to a low $\Delta\rho/\eta$. In contrast, the viscosity minimum, i.e., ∼6−10 GPa or ∼180−200 km depth, leads to maxima in $\Delta\rho/\eta$ ratios. Thus, at the depths where $\Delta\rho/\eta$ shows a maxima, the melt fraction is expected to be at a minimum because the melt is likely to migrate out if the mantle is permeable.[20,84,94] At shallower depths of ∼90−100 km, where magma is more viscous compared to deeper parts of the Earth, the magma mobility $\Delta\rho/\eta$ is likely to be low and likely to create ponding of the partial melts, which might be the source for the seismically observed low velocity at the lithosphere−asthenosphere boundary (LAB).[1,2,4] The viscosity of anhydrous and hydrous aluminosilicate melts is likely to be applicable for estimating the mobility of the ascending magma in subduction zone settings and also the stability and buoyancy of possible partial melts trapped at the LAB.[3]

■ ASSOCIATED CONTENT

Supporting Information

The Supporting Information is available free of charge on the ACS Publications website at DOI: 10.1021/acsearthspacechem.8b00157.

Supplementary Text S-1, Figures S-1−S-4, and Tables S-1 and S-2 (PDF)

Supplementary Datasets 1−5 (XLSX)

■ AUTHOR INFORMATION

Corresponding Author

*E-mail: mmookherjee@fsu.edu.

ORCID

Suraj K. Bajgain: 0000-0002-8923-8247

Mainak Mookherjee: 0000-0002-0605-5964

Notes

The authors declare no competing financial interest.

■ ACKNOWLEDGMENTS

The authors thank Alisha N. Clark, Bouhifd Ali, and an anonymous reviewer for their constructive criticism, which helped in enhancing the clarity of the manuscript. Mainak Mookherjee acknowledges the National Science Foundation grant (EAR1763215 and EAR1753125) and Ralph E. Powe Junior Faculty Enhancement Award from the Oak Ridge Associated University (ORAU). The authors also acknowledge the Extreme Science and Engineering Discovery Environment (XSEDE) supercomputing facilities and the Research Computing Center (RCC) at Florida State University (FSU) for computing resources. Matthew Solomon acknowledges the Young Scholar Program at FSU.

DOI: 10.1021/acsearthspacechem.8b00157
ACS Earth Space Chem. 2019, 3, 390−402

REFERENCES

(1) Schmerr, N. The Gutenberg discontinuity: Melt at the lithosphere-asthenosphere boundary. *Science* **2012**, *335* (6075), 1480−1483.
(2) Naif, S.; Key, K.; Constable, S.; Evans, R. Melt-rich channel observed at the lithosphere-asthenosphere boundary. *Nature* **2013**, *495* (7441), 356−359.
(3) Crépisson, C.; Morard, G.; Bureau, H.; Prouteau, G.; Morizet, Y.; Petitgirard, S.; Sanloup, C. Magmas trapped at the continental lithosphere−asthenosphere boundary. *Earth Planet. Sci. Lett.* **2014**, *393*, 105−112.
(4) Chantel, J.; Manthilake, G.; Andrault, D.; Novella, D.; Yu, T.; Wang, Y. Experimental evidence supports mantle partial melting in the asthenosphere. *Science advances* **2016**, *2* (5), No. e1600246.
(5) Toffelmier, D. A.; Tyburczy, J. A. Electromagnetic detection of a 410-km-deep melt layer in the southwestern United States. *Nature* **2007**, *447* (7147), 991−994.
(6) Tauzin, B.; Debayle, E.; Wittlinger, G. Seismic evidence for a global low-velocity layer within the Earth's upper mantle. *Nat. Geosci.* **2010**, *3* (10), 718−721.
(7) Schmandt, B.; Jacobsen, S. D.; Becker, T. W.; Liu, Z.; Dueker, K. G. Dehydration melting at the top of the lower mantle. *Science* **2014**, *344* (6189), 1265−1268.
(8) Revenaugh, J.; Sipkin, S. A. Seismic evidence for silicate melt atop the 410-km mantle discontinuity. *Nature* **1994**, *369*, 474−476.
(9) Bercovici, D.; Karato, S. Whole mantle convection and the transition-zone water filter. *Nature* **2003**, *425*, 39−44.
(10) Freitas, D.; Manthilake, G.; Schiavi, F.; Chantel, J.; Bolfan-Casanova, N.; Bouhifd, M. A.; Andrault, D. Experimental evidence supporting a global melt layer at the base of the Earth's upper mantle. *Nat. Commun.* **2017**, *8* (1), 2186.
(11) Williams, Q.; Garnero, E. J. Seismic evidence for partial melt at the base of Earth's mantle. *Science* **1996**, *273*, 1528−1530.
(12) Stixrude, L.; Karki, B. Structure and freezing of $MgSiO_3$ liquid in Earth's lower mantle. *Science* **2005**, *310* (5746), 297−299.
(13) Kushiro, I. Changes in viscosity and structure of melt of $NaAlSi_2O_6$ composition at high pressures. *J. Geophys. Res.* **1976**, *81* (35), 6347−6350.
(14) Poe, B. T.; McMillan, P. F.; Rubie, D. C.; Chakraborty, S.; Yarger, J.; Diefenbacher, J. Silicon and oxygen self-diffusivities in silicate liquids measured to 15 gigapascals and 2800 Kelvin. *Science* **1997**, *276* (5316), 1245−1248.
(15) Dingwell, D. B. Melt viscosity and diffusion under elevated pressures. *Rev. Mineral. Geochem.* **1998**, *37* (1), 397−424.
(16) Tinker, D.; Lesher, C. E.; Hutcheon, I. D. Self-diffusion of Si and O in diopside-anorthite melt at high pressures. *Geochim. Cosmochim. Acta* **2003**, *67* (1), 133−142.
(17) Tinker, D.; Lesher, C. E.; Baxter, G. M.; Uchida, T.; Wang, Y. High-pressure viscometry of polymerized silicate melts and limitations of the Eyring equation. *Am. Mineral.* **2004**, *89* (11−12), 1701−1708.
(18) Suzuki, A.; Ohtani, E.; Terasaki, H.; Nishida, K.; Hayashi, H.; Sakamaki, T.; Shibazaki, Y.; Kikegawa, T. Pressure and temperature dependence of the viscosity of a $NaAlSi_2O_6$ melt. *Phys. Chem. Miner.* **2011**, *38* (1), 59−64.
(19) Bauchy, M.; Guillot, B.; Micoulaut, M.; Sator, N. Viscosity and viscosity anomalies of model silicates and magmas: A numerical investigation. *Chem. Geol.* **2013**, *346*, 47−56.
(20) Wang, Y.; Sakamaki, T.; Skinner, L. B.; Jing, Z.; Yu, T.; Kono, Y.; Park, C.; Shen, G.; Rivers, M. L.; Sutton, S. R. Atomistic insight into viscosity and density of silicate melts under pressure. *Nat. Commun.* **2014**, *5*, 3241.
(21) Reid, J. E.; Poe, B. T.; Rubie, D. C.; Zotov, N.; Wiedenbeck, M. The self-diffusion of silicon and oxygen in diopside ($CaMgSi_2O_6$) liquid up to 15 GPa. *Chem. Geol.* **2001**, *174* (1), 77−86.
(22) Reid, J. E.; Suzuki, A.; Funakoshi, K.-I.; Terasaki, H.; Poe, B. T.; Rubie, D. C.; Ohtani, E. The viscosity of $CaMgSi_2O_6$ liquid at pressures up to 13 GPa. *Phys. Earth Planet. Inter.* **2003**, *139* (1), 45−54.
(23) Cochain, B.; Sanloup, C.; Leroy, C.; Kono, Y. Viscosity of mafic magmas at high pressures. *Geophys. Res. Lett.* **2017**, *44* (2), 818−826.
(24) Posner, E. S.; Schmickler, B.; Rubie, D. C. Self-diffusion and chemical diffusion in peridotite melt at high pressure and implications for magma ocean viscosities. *Chem. Geol.* **2018**, *502*, 66−75.
(25) White, B. S.; Montana, A. The effect of H2O and CO2 on the viscosity of sanidine liquid at high pressures. *J. Geophys. Res.* **1990**, *95* (B10), 15683−15693.
(26) Whittington, A.; Richet, P.; Holtz, F. Water and the viscosity of depolymerized aluminosilicate melts. *Geochim. Cosmochim. Acta* **2000**, *64*, 3725−3736.
(27) Mysen, B. Water-melt interaction in hydrous magmatic systems at high temperature and pressure. *Progress in Earth and Planetary Science* **2014**, *1* (1), 4.
(28) Karki, B. B.; Bhattarai, D.; Stixrude, L. First-principles simulations of liquid silica: Structural and dynamical behavior at high pressure. *Phys. Rev. B: Condens. Matter Mater. Phys.* **2007**, *76* (10), 104205.
(29) Lacks, D. J.; Rear, D. B.; Van Orman, J. A. Molecular dynamics investigation of viscosity, chemical diffusivities and partial molar volumes of liquids along the $MgO-SiO_2$ join as functions of pressure. *Geochim. Cosmochim. Acta* **2007**, *71* (5), 1312−1323.
(30) Guillot, B.; Sator, N. A computer simulation study of natural silicate melts. Part II: High pressure properties. *Geochim. Cosmochim. Acta* **2007**, *71* (18), 4538−4556.
(31) Karki, B. B.; Bohara, B.; Stixrude, L. First-principles study of diffusion and viscosity of anorthite ($CaAl_2Si_2O_8$) liquid at high pressure. *Am. Mineral.* **2011**, *96* (5−6), 744−751.
(32) Ni, H.; de Koker, N. Thermodynamics, diffusion and structure of $NaAlSi_2O_6$ liquid at mantle conditions: A first-principles molecular dynamics investigation. *J. Geophys. Res.: Solid Earth* **2011**, *116* (B9), B09202.
(33) Kresse, G.; Hafner, J. Ab initio molecular dynamics for liquid metals. *Phys. Rev. B: Condens. Matter Mater. Phys.* **1993**, *47* (1), 558−561.
(34) Kresse, G.; Furthmüller, J. Efficiency of ab-initio total energy calculations for metals and semiconductors using a plane-wave basis set. *Comput. Mater. Sci.* **1996**, *6* (1), 15−50.
(35) Kresse, G.; Furthmüller, J. Efficient iterative schemes for ab initio total-energy calculations using a plane-wave basis set. *Phys. Rev. B: Condens. Matter Mater. Phys.* **1996**, *54* (16), 11169.
(36) Kresse, G.; Joubert, D. From ultrasoft pseudopotentials to the projector augmented-wave method. *Phys. Rev. B: Condens. Matter Mater. Phys.* **1999**, *59*, 1758−1775.
(37) Nosé, S. A unified formulation of the constant temperature molecular dynamics methods. *J. Chem. Phys.* **1984**, *81* (1), 511−519.
(38) Flyvbjerg, H.; Petersen, H. G. Error estimates on averages of correlated data. *J. Chem. Phys.* **1989**, *91* (1), 461−466.
(39) Lange, R. A.; Carmichael, I. S. Densities of Na_2O-K_2O-MgO-FeO-Fe_2O_3-Al_2O_3-TiO_2-SiO_2 liquids: New measurements and derived partial molar properties. *Geochim. Cosmochim. Acta* **1987**, *51*, 2931−2946.
(40) Lange, R. A. A revised model for the density and thermal expansivity of K_2O-Na_2O-CaO-MgO-Al_2O_3-SiO_2 liquids from 700 to 1900 K: Extension to crustal magmatic temperatures. *Contrib. Mineral. Petrol.* **1997**, *130* (1), 1−11.
(41) Sakamaki, T. Density of jadeite melts under high pressure and high temperature conditions. *J. Mineral. Petrol. Sci.* **2017**, *112* (5), 300−307.
(42) Mookherjee, M.; Stixrude, L.; Karki, B. Hydrous silicate melt at high pressure. *Nature* **2008**, *452*, 983−986.
(43) Bajgain, S.; Ghosh, D. B.; Karki, B. B. Structure and density of basaltic melts at mantle conditions from first-principles simulations. *Nat. Commun.* **2015**, *6*, 8578.
(44) Ghosh, D. B.; Bajgain, S. K.; Mookherjee, M.; Karki, B. B. Carbon-bearing silicate melt at deep mantle conditions. *Sci. Rep.* **2017**, *7*, 1−8.
(45) Allen, M.; Tildesley, D. *Computer Simulation of Liquids*; Clarendon Press: Oxford, U.K., 1987.

DOI: 10.1021/acsearthspacechem.8b00157
ACS Earth Space Chem. 2019, 3, 390−402

(46) Daivis, P. J.; Evans, D. J. Comparison of constant pressure and constant volume nonequilibrium simulations of sheared model decane. *J. Chem. Phys.* **1994**, *100* (1), 541−547.
(47) Nevins, D.; Spera, F. Accurate computation of shear viscosity from equilibrium molecular dynamics simulations. *Mol. Simul.* **2007**, *33* (15), 1261−1266.
(48) Chen, T.; Smit, B.; Bell, A. T. Are pressure fluctuation-based equilibrium methods really worse than nonequilibrium methods for calculating viscosities? *J. Chem. Phys.* **2009**, *131* (24), 246101.
(49) Ochs, F. A., III; Lange, R. A. The partial molar volume, thermal expansivity, and compressibility of H_2O in $NaAlSi_3O_8$ liquid: New measurements and an internally consistent model. *Contrib. Mineral. Petrol.* **1997**, *129* (2−3), 155−165.
(50) Bouhifd, M.; Whittington, A.; Richet, P. Densities and volumes of hydrous silicate melts: New measurements and predictions. *Chem. Geol.* **2015**, *418*, 40−50.
(51) Pitzer, K. S.; Sterner, S. M. Equations of state valid continuously from zero to extreme pressures for H_2O and CO_2. *J. Chem. Phys.* **1994**, *101* (4), 3111−3116.
(52) Burnham, C. W.; Davis, N. F. The role of H_2O in silicate melts: I. P−V−T relations in the system $NaAlSi_3O_8$ -H_2O to 10 kilobars and 1000 °C. *Am. J. Sci.* **1971**, *270*, 54−79.
(53) Agee, C. B. Static compression of hydrous silicate melt and the effect of water on planetary differentiation. *Earth Planet. Sci. Lett.* **2008**, *265* (3), 641−654.
(54) Jing, Z.; Karato, S.-i. Effect of H2O on the density of silicate melts at high pressures: Static experiments and the application of a modified hard-sphere model of equation of state. *Geochim. Cosmochim. Acta* **2012**, *85*, 357−372.
(55) Sakamaki, T.; Ohtani, E.; Urakawa, S.; Suzuki, A.; Katayama, Y. Measurement of hydrous peridotite magma density at high pressure using the X-ray absorption method. *Earth Planet. Sci. Lett.* **2009**, *287* (3−4), 293−297.
(56) Matsukage, K. N.; Jing, Z.; Karato, S. Density of hydrous silicate melt at the conditions of Earth's deep upper mantle. *Nature* **2005**, *438* (7067), 488−491.
(57) Sakamaki, T.; Suzuki, A.; Ohtani, E. Stability of hydrous melt at the base of the Earth's upper mantle. *Nature* **2006**, *439*, 192−194.
(58) Malfait, W. J.; Seifert, R.; Petitgirard, S.; Perrillat, J.-P.; Mezouar, M.; Ota, T.; Nakamura, E.; Lerch, P.; Sanchez-Valle, C. Supervolcano eruptions driven by melt buoyancy in large silicic magma chambers. *Nat. Geosci.* **2014**, *7* (2), 122−125.
(59) Malfait, W. J.; Seifert, R.; Petitgirard, S.; Mezouar, M.; Sanchez-Valle, C. The density of andesitic melts and the compressibility of dissolved water in silicate melts at crustal and upper mantle conditions. *Earth Planet. Sci. Lett.* **2014**, *393*, 31−38.
(60) Karki, B. B. First-principles molecular dynamics simulations of silicate melts: Structural and dynamical properties. *Rev. Mineral. Geochem.* **2010**, *71*, 355−389.
(61) Sakamaki, T. Density of hydrous magma. *Chem. Geol.* **2017**, *475*, 135−139.
(62) Zhang, L.; Van Orman, J. A.; Lacks, D. J. Molecular dynamics investigation of MgO−CaO−SiO_2 liquids: Influence of pressure and composition on density and transport properties. *Chem. Geol.* **2010**, *275* (1), 50−57.
(63) Ni, H.; Hui, H.; Steinle-Neumann, G. Transport properties of silicate melts. *Rev. Geophys.* **2015**, *53* (3), 715−744.
(64) Chakraborty, S. Diffusion in silicate melts. *Reviews in Mineralogy and Geochemistry* **1995**, *32* (1), 411−503.
(65) Angell, C. A.; Cheeseman, P. A.; Tamaddon, S. Pressure enhancement of ion mobilities in liquid silicates from computer simulation studies to 800 kilobars. *Science* **1982**, *218* (4575), 885−887.
(66) Lesher, C.; Hervig, R.; Tinker, D. Self diffusion of network formers (silicon and oxygen) in naturally occurring basaltic liquid. *Geochim. Cosmochim. Acta* **1996**, *60* (3), 405−413.
(67) Tinker, D.; Lesher, C. E. Self diffusion of Si and O in dacitic liquid at high pressures. *Am. Mineral.* **2001**, *86* (1−2), 1−13.
(68) Shimizu, N.; Kushiro, I. Diffusivity of oxygen in jadeite and diopside melts at high pressures. *Geochim. Cosmochim. Acta* **1984**, *48* (6), 1295−1303.
(69) Bryce, J. G.; Spera, F. J.; Stein, D. J. Pressure dependence of self-diffusion in the $NaAlO_2$-SiO_2 system: Compositional effects and mechanisms. *Am. Mineral.* **1999**, *84* (3), 345−356.
(70) Karki, B. B.; Bhattarai, D.; Mookherjee, M.; Stixrude, L. Visualization-based analysis of structural and dynamical properties of simulated hydrous silicate melt. *Phys. Chem. Miner.* **2010**, *37* (2), 103−117.
(71) Karki, B. B.; Stixrude, L. First-principles study of enhancement of transport properties of silica melt by water. *Phys. Rev. Lett.* **2010**, *104* (21), 744−751.
(72) Silver, L.; Stolper, E. Water in albitic glasses. *J. Petrol.* **1989**, *30* (3), 667−709.
(73) Dixon, J. E.; Stolper, E. M. An experimental study of water and carbon dioxide solubilities in mid-ocean ridge basaltic liquids. Part II: Applications to degassing. *J. Petrol.* **1995**, *36* (6), 1633−1646.
(74) Makhluf, A.; Newton, R.; Manning, C. Hydrous albite magmas at lower crustal pressure: New results on liquidus H_2O content, solubility, and H_2O activity in the system $NaAlSi_3O_8$−H_2O−NaCl at 1.0 GPa. *Contrib. Mineral. Petrol.* **2016**, *171* (8−9), 75.
(75) Verma, A. K.; Karki, B. B. First-principles study of self-diffusion and viscous flow in diopside ($CaMgSi_2O_6$) liquid. *Am. Mineral.* **2012**, *97* (11−12), 2049−2055.
(76) Hess, K.; Dingwell, D. Viscosities of hydrous leucogranitic melts: A non-Arrhenian model. *Am. Mineral.* **1996**, *81* (9−10), 1297−1300.
(77) Giordano, D.; Dingwell, D. B. Non-Arrhenian multicomponent melt viscosity: A model. *Earth Planet. Sci. Lett.* **2003**, *208* (3−4), 337−349.
(78) Giordano, D.; Russell, J. K.; Dingwell, D. B. Viscosity of magmatic liquids: A model. *Earth Planet. Sci. Lett.* **2008**, *271* (1), 123−134.
(79) Funakoshi, K.-i.; Suzuki, A.; Terasaki, H. In situ viscosity measurements of albite melt under high pressure. *J. Phys.: Condens. Matter* **2002**, *14* (44), 11343.
(80) Suzuki, A.; Ohtani, E.; Terasaki, H.; Funakoshi, K.-i. Viscosity of silicate melts in $CaMgSi_2O_6$−$NaAlSi_2O_6$ system at high pressure. *Phys. Chem. Miner.* **2005**, *32* (2), 140−145.
(81) Le Roux, S.; Petkov, V. ISAACS−interactive structure analysis of amorphous and crystalline systems. *J. Appl. Crystallogr.* **2010**, *43* (1), 181−185.
(82) Sakamaki, T.; Wang, Y.; Park, C.; Yu, T.; Shen, G. Contrasting behavior of intermediate-range order structures in jadeite glass and melt. *Phys. Earth Planet. Inter.* **2014**, *228*, 281−286.
(83) Inamura, Y.; Katayama, Y.; Utsumi, W.; Funakoshi, K.-i. Transformations in the Intermediate-Range Structure of SiO_2 Glass under High Pressure and Temperature. *Phys. Rev. Lett.* **2004**, *93* (1), 015501.
(84) Sakamaki, T.; Suzuki, A.; Ohtani, E.; Terasaki, H.; Urakawa, S.; Katayama, Y.; Funakoshi, K.-i.; Wang, Y.; Hernlund, J. W.; Ballmer, M. D. Ponded melt at the boundary between the lithosphere and asthenosphere. *Nat. Geosci.* **2013**, *6* (12), 1041−1044.
(85) Ohtani, E.; Taulelle, F.; Angell, C. A. Al^{3+} coordination changes in liquid aluminosilicates under pressure. *Nature* **1985**, *314* (6006), 78−81.
(86) Stebbins, J. F.; Xu, Z. NMR evidence for excess non-bridging oxygen in an aluminosilicate glass. *Nature* **1997**, *390* (6655), 60−62.
(87) Mysen, B. O.; Richet, P. *Silicate Glasses and Melts: Properties and Structure*; Elsevier: Amsterdam, Netherlands, 2005; Vol. *10*.
(88) Allwardt, J. R.; Stebbins, J. F.; Terasaki, H.; Du, L.-S.; Frost, D. J.; Withers, A. C.; Hirschmann, M. M.; Suzuki, A.; Ohtani, E. Effect of structural transitions on properties of high-pressure silicate melts: ^{27}Al NMR, glass densities, and melt viscosities. *Am. Mineral.* **2007**, *92* (7), 1093−1104.
(89) Angell, C. A. Formation of glasses from liquids and biopolymers. *Science* **1995**, *267* (5206), 1924−1935.

DOI: 10.1021/acsearthspacechem.8b00157
ACS Earth Space Chem. 2019, 3, 390−402

(90) Yarger, J.; Smith, K.; Nieman, R.; Diefenbacher, J.; Wolf, G.; Poe, B.; McMillan, P. Al coordination changes in high-pressure aluminosilicate liquids. *Science* **1995**, *270*, 1964−1967.
(91) Toplis, M. J.; Dingwell, D. B. Shear viscosities of CaO-Al_2O_3-SiO_2 and MgO-Al_2O_3-SiO_2 liquids: Implications for the structural role of aluminium and the degree of polymerization of synthetic and natural aluminosilicate melts. *Geochim. Cosmochim. Acta* **2004**, *68* (24), 5169−5188.
(92) Whittington, A. G.; Bouhifd, M. A.; Richet, P. Amorphous Materials: Properties, Structure, and Durability: The viscosity of hydrous $NaAlSi_3O_8$ and granitic melts: Configurational entropy models. *Am. Mineral.* **2009**, *94* (1), 1−16.
(93) Stolper, E.; Walker, D.; Hager, B. H.; Hays, J. F. Melt segregation from partially molten source regions: The importance of melt density and source region size. *J. Geophys. Res.: Solid Earth* **1981**, *86* (B7), 6261−6271.
(94) Connolly, J. A.; Schmidt, M. W.; Solferino, G.; Bagdassarov, N. Permeability of asthenospheric mantle and melt extraction rates at mid-ocean ridges. *Nature* **2009**, *462* (7270), 209−212.
(95) Duffy, T. S.; Anderson, D. L. Seismic velocities in mantle minerals and the mineralogy of the upper mantle. *J. Geophys. Res.* **1989**, *94* (B2), 1895−1912.
(96) Stixrude, L.; Lithgow-Bertelloni, C. Thermodynamics of mantle minerals−I. Physical properties. *Geophys. J. Int.* **2005**, *162* (2), 610−632.
(97) Jing, Z.; Karato, S.-i. Compositional effect on the pressure derivatives of bulk modulus of silicate melts. *Earth Planet. Sci. Lett.* **2008**, *272* (1−2), 429−436.
(98) Sanloup, C.; Drewitt, J. W.; Konôpková, Z.; Dalladay-Simpson, P.; Morton, D. M.; Rai, N.; van Westrenen, W.; Morgenroth, W. Structural change in molten basalt at deep mantle conditions. *Nature* **2013**, *503* (7474), 104−107.

DOI: 10.1021/acsearthspacechem.8b00157
ACS Earth Space Chem. 2019, 3, 390−402